AEROSPACE REPORT NO.
ATR-2022-00960

Using Continuous Slowing Down Approximation and the Right Parallel Piped Model to Estimate Single Event Effects Rates

March 31, 2022

T. Paul O'Brien
Space Sciences Department
Space Science Applications Laboratory

Prepared for:
Space Hazards Applications, LLC
1909 Arapahoe Street
Golden, CO 80401

Contract No. SHA-189

Authorized by: Engineering and Technology Group

Acknowledgments

The author acknowledges useful discussions with J. Green of Space Hazards and S. Messenger of Northrop Grumman. The MIT Lincoln Laboratory LLASEE tool documentation by J.B. Parham et al. also provided a valuable survey of the relevant literature. M. Worstell of The Aerospace Corporation provided the SRIM data tables, and S. Davis of Aerospace provided the CREME96 runs.

Abstract

This report describes the equations and calculations needed to compute the single-event effect (SEE) rate for parts inside slab or spherical shielding. We use the continuous slowing-down approximation (CSDA) to compute a degraded spectrum emerging from shielding (e.g., aluminum). For proton-sensitive parts, we convolve the degraded spectrum with the Weibull response function. For ion-sensitive parts, we convert the degraded ion energy spectrum into a computed linear energy transfer (LET) spectrum, then convolve the LET spectrum with the Weibull response function, including a correction for the asymmetric shape of the part using the right parallel piped (RPP) model. We express the calculations as both integrals and discrete sums and make recommendations on the best approach for interpolation and numerical derivatives. The discrete sum weights can be captured as tensors so that they can be reused for multiple flux spectra.

Contents

Figures

Tables

1. Introduction

It is a common problem in the study of single-event effects (SEEs) to estimate the SEE rate given a particle flux. The broadest statement of this problem begins with an ion energy spectrum representing multiple ion species. First, this incident spectrum must be propagated through shielding, producing a degraded ion energy spectrum. For our purposes, the continuous slowing-down approximation (CSDA) is often adequate (it is often good for ions, rarely good for electrons). In this approximation, we use the range as a function of energy in the shielding material for each ion to determine how much energy is lost traveling through the shield. We do this for spherical and slab shielding; in the latter case, there is a distribution of path lengths through the shield that must be addressed by an extra integral.

Next, the degraded ion energy spectrum must be converted into a linear energy transfer (LET) spectrum, which consolidates all the ion fluxes into a single spectrum. Finally, the LET spectrum is convolved with the part cross section to obtain an SEE rate. For ion-sensitive parts, it is necessary to correct for the asymmetric shape of the sensitive volume: laboratory test data are taken at normal incident through what is often the thinnest dimension of the part. Parts are approximated as being box shaped or, formally, a right parallel piped (RPP). The dimensions of the RPP can be obtained from test data and some assumptions about the part (thickness, aspect ratio).

For proton-sensitive parts, it is only necessary to degrade the incident spectrum and convolve that result with the laboratory cross section. Proton SEE rates do not depend on the geometry of the sensitive volume, only its total volume (number of nuclear targets). This is because protons do not directly cause SEE, but rather collide with nuclei in the part, producing short-range, high LET energetic heavy ions inside the part. In Reference [[1]] we described the proton SEE rate calculation in much the same way as presented here. Two excellent general resources for SEE rate calculations are [[2]] and [[3]], covering all the concepts presented here.

With this information in hand, we can walk through the various calculations: degraded flux, LET spectrum, and SEE rate.

2. Computing Degraded Flux

The CSDA approximation (e.g., [[4]]) states that, for particles passing through a range T of shielding:

$$J'_{out,>}(R_{out}) = J'_{in,>}(R_{out} + T) = J'_{in,>}(R_{in}) \tag{1}$$

where $J'_{out,>}$ is the flux of particles exiting the shield with range greater than R_{out}, and $J'_{in,>}$ is the flux of particles entering the shield with range greater than R_{in}. That is, particles lose range T passing through the shield. In terms of differential flux $j'(T) = -\frac{d}{dT}J'_{>}(T)$, the degraded energy spectrum is:

$$j'_{out}(R_{out}) = j'_{in}(R_{out} + T') = j'_{in}(R_{in}) \tag{2}$$

However, we do not normally represent flux as a function of range. Rather, we have integral and differential flux with respect to energy (an energy spectrum). To convert from an integral range spectrum to an energy spectrum, we need the range energy table, which provides $R(E)$, the range for particles of a given species in a given shield material as a function of incident energy E. With this function, we can write:

$$J'_{>}(R(E)) = J_{>}(E) \tag{3}$$

where $J_{>}(E)$ (without the prime) is the flux of particles with energy greater than E and typically has units like #/cm^2/s. Thus, using the same notation conventions, the equation for transport of an integral energy spectrum through shielding is:

$$J_{out,>}(E_{out}) = J_{in,>}\left(R^{-1}(R(E_{out}) + T)\right) = J_{in,>}(E_{in}) \tag{4}$$

In terms of differential flux $j(E) = -\frac{d}{dE}J_{>}(E)$, which has units like #/cm^2/s/MeV, the degraded energy spectrum is:

$$j_{out}(E_{out}) = j_{in}\left(E_{in}(E_{out};T)\right)\left(\left.\frac{dR}{dE}\right|_{E_{in}(E_{out};T)}\right)^{-1}\left.\frac{dR}{dE}\right|_{E_{out}} \tag{5}$$

where we have treated the incident energy E_{in} as a function of the exit energy E_{out} and the shielding thickness T: $E_{in}(E_{out};T) = R^{-1}(R(E_{out}) + T)$. The chain rule leads to the two factors containing $\frac{dR}{dE}$. For a sphere with uniform thickness T, this formula provides the conversion from incident to exit differential energy flux. We can discretize it on an energy grid E_k as a matrix-vector operation using the following approach:

$$\vec{J}_{out} = \underline{D}\vec{J}_{in}$$

$$j_{out}(E_k) = \sum_{k'} D_{k,k'} j_{in}(E_{k'})$$

$$D_{k,k'} = \left.\frac{dR}{dE}\right|_{E_k}\left(\left.\frac{dR}{dE}\right|_{E_{in}(E_k;T)}\right)^{-1} A(\ln E_{in}(E_k;T), \ln E_{k'})$$

If we have to compute $\frac{dR}{dE}$ numerically, it is computed from the range-energy table as $\frac{R_k}{E_k}\frac{d\ln R_k}{d\ln E_k}$, using:

$$\left.\frac{dR}{dE}\right|_{E_k} = \frac{R_k}{E_k}\frac{d\ln R_k}{d\ln E_k} \tag{6}$$

$$\frac{d\ln R_k}{d\ln E_k} = \begin{cases} \frac{\ln R_2 - \ln R_1}{\ln E_2 - \ln E_1} & k = 1 \\ \frac{\ln R_{k+1} - \ln R_{k-1}}{\ln E_{k+1} - \ln E_{k-1}} & 1 < k < N_k \\ \frac{\ln R_N - \ln R_{N-1}}{\ln E_N - \ln E_{N-1}} & k = N_k \end{cases} \tag{7}$$

This type of log-log derivative is numerically more stable than a linear derivative on values that range over orders of magnitude.

The interpolating matrix A interpolates flux from derived incident energy $E_{in}(E_k;T)$ to its corresponding output energy E_k, and we do it in a log sense to improve numerical performance on energy that spans orders of magnitude. The general form of the interpolating matrix is:

$$A(x_i,x_j) = \begin{cases} \frac{x_{j+1}-x_i}{x_{j+1}-x_j} & x_j \le x_i < x_{j+1}\ ;\ j < N_j \\ \frac{x_i - x_{j-1}}{x_j - x_{j-1}} & x_{j-1} \le x_i < x_j\ ;\ j > 1 \\ 0 & \text{otherwise} \end{cases} \tag{8}$$

$$f(x_i) \approx \sum_j A(x_i,x_j)\, f(x_j) \tag{9}$$

The degraded weight matrix $\underline{\underline{D}}$ converts from incident to degraded flux. It is efficient to precompute the $\underline{\underline{D}}$ on the energy grid of the range table, and so we will identify that as E_k. However, in practice, the working energy grid E_i is not the same as E_k. The interpolation between the two can be performed in what we call "smart" interpolation: it uses linear interpolation in log flux versus log energy sense for points in the output grid where neighboring fluxes on the input grid are nonzero and linear interpolation in flux versus log energy otherwise. We implement smart interpolation by performing both interpolations and using the former wherever it is finite (i.e., no zeros produced infinite or not-a-number results) and the latter otherwise. This type of interpolation is not appropriate when there is need to store the interpolation weights for future reuse; in those cases, an interpolating matrix A should be used, usually constructed from log energy grids.

Next, we consider the case of slab geometry, where there is a distribution $K(T';T)$ of path lengths through the shield. In this case, we can integrate the differential range spectrum:

$$j'_{out}(R_{out}) = \int j'_{in}(R_{in})K(T';T)dT' = \int j'_{in}(R_{out}+T')K(T';T)dT' \tag{10}$$

This integral is independent of $R(E)$ and will be used when we discretize the problem. In terms of differential energy spectra, the solution is:

$$j_{out}(E_{out}) = \left.\frac{dR}{dE}\right|_{E_{out}} \int j_{in}\big(E_{in}(E_{out};T')\big)\left(\left.\frac{dR}{dE}\right|_{E_{in}(E_{out};T')}\right)^{-1} K(T';T)T'd\ln T' \tag{11}$$

For a sphere of thickness T, $K(T';T) = \delta(T' - T)$, and the integrals simplify to (5). However, for a slab of thickness T, the path length distribution is:

$$K(T';T) = \frac{1}{2}\int_0^{\pi/2} \delta\left(T' - \frac{T}{\cos\theta}\right)\sin\theta\, d\theta = \frac{1}{2}\frac{\sin\theta}{|dT'/d\theta|} = \frac{\cos^2\theta}{2T} = \begin{cases} 0 & T' < T \\ \frac{T}{2T'^2} & T' \geq T \end{cases} \tag{12}$$

The integral over θ accounts for secant effects that create longer path lengths through the slab. The ½ factor out front arises from the fact that slab geometry is usually treated as coming only from one hemisphere (one side off the slab) rather than the full 4π sr assumed in the spherically symmetric case.

In the discrete form, we first capture the species-independent integral in a matrix $\underline{\underline{Q}}$:

$$Q_{m,m''} = \int_T^\infty A(\ln(T_m + T')\,, \ln T_{m''})K(T';T)dT' \tag{13}$$

We can compute the integral numerically using an algorithm like adaptive quadrature, in which case we should compact the bounds of integration for any given m'':

$$Q_{m,m''} = Q_{m,m''} = \int_{T_{\max(1,m''-1)}}^{T_{\min(N_m,m''+1)}} A(\ln(T_m + T')\,, \ln T_{m''})K(T';T)dT' \tag{14}$$

where N_m is the number of grid points in the T_m grid. Because of this narrow range of integration, it is not necessary to convert the integral to $d\ln T'$.

Alternatively, we can use the trapezoidal integration rule:

$$Q_{m,m''} = \sum_{m'} A(\ln(T_m + T_{m'})\,, \ln T_{m''})K(T_{m'};T)\Delta T_{m'} \tag{15}$$

Here $\Delta T_{m'}$ are trapezoidal integral weights:

$$\Delta T_m = \begin{cases} \frac{T_{m+1} - T_m}{2} & j = 1 \\ \frac{T_{m+1} - T_{m-1}}{2} & 1 < m < N_m \\ \frac{T_m - T_{m-1}}{2} & m = N_m \end{cases} \tag{16}$$

To compute the degraded weight matrix for a particular species, we have:

$$\underline{\underline{D_s}} = \text{diag}\left(\left.\frac{dR_s}{dE}\right|_{E_k}\right)\underline{\underline{A_s}}\,\underline{\underline{Q}}\,\underline{\underline{A'}}_s\,\text{diag}\left(\left(\left.\frac{dR_s}{dE}\right|_{E_{k'}}\right)^{-1}\right) \tag{17}$$

$$\underline{\underline{A_s}} = A(\ln R_k\,, \ln T_m) \tag{18}$$

$$\underline{\underline{A'}}_s = A(\ln T_m\,, \ln R_k) \sim \underline{\underline{A_s}}^T \tag{19}$$

where the subscripts s clarify which factors are species-specific and which ones are not. Note that the energy grid E_k is usually also species specific. Likewise, the spherical weights and grids are also species specific. With $\underline{\underline{D_s}}$ in hand for spherical or slab geometry, we can quickly convert incident flux to degraded flux: we smart interpolate the incident flux from the E_i to the E_k, apply $\vec{j}_{s,out} = \underline{\underline{D_s}}\vec{j}_{s,in}$ and smart

interpolate $\vec{J}_{s,out}$ back onto the E_i grid. Next, we will address how to convert (degraded) flux to an LET spectrum.

3. Computing an LET spectrum

For ion-sensitive parts, the SEE rate is computed from an LET spectrum, which consolidates all the individual (degraded) ion energy spectra into a single spectrum versus LET. It is recommended to exclude protons from the LET spectrum for two reasons. First, it is very rare for parts to be upset by direct ionization from protons. Second, protons with high LET also have very short range such that they can lose a significant fraction of their incident energy or even stop in the sensitive volume, and the approximations given here do not account for change of LET or stopping while passing through the sensitive volume. As discussed above, protons do cause SEE but via knock-on nuclei rather than direct ionization. That will be treated in the next section. The LET spectrum is:

$$j_L(L) = \sum_s \sum_{E_L:L_s(E_L)=L} j_s(E_L) \left|\frac{dL_s}{dE}\right|_{E_L}^{-1} \tag{20}$$

Here $j_L(L)$ is the differential spectrum with respect to LET (L), which has units like #/cm^2/s/(MeV/(g/cm^2)), j_s is the incident or degraded flux for species s, and L_s is its LET function:

$$L_s(E) = \left(\left.\frac{dR_s}{dE}\right|_E\right)^{-1} \tag{21}$$

Because $L_s(E)$ is not monotonic, the inner sum is taken over all monotonic segments of $L_s(E)$ that have a point E_L with $L_s(E_L) = L$. To perform this calculation numerically, we first compute $\left.\frac{dR_s}{dE}\right|_E$ using the log-log method on the range table's energy grid (E_k). We then interpolate that onto the E_i grid using log-log interpolation (this step is not needed if the E_i grid is the E_k grid). Next, we break $L_s(E_i)$ into n monotonic segments. Segments with zero slope are omitted. Within each segment, we compute $\frac{dL_s}{dE}$ numerically using the log-log method. Because we have $L_i = L_s(E_i)$, and it is monotonic within a segment, we can treat $\frac{dL_s}{dE}$ as a function of L_i or E_i. We therefore can simply interpolate $\frac{dL_s}{dE}$ in a log-log sense onto the desired output L. This defines E_L implicitly; segments whose range of L does not include the output L do not contribute to $j_L(L)$.

To capture this transform numerically, we write:

$$j_L(L_m) \approx \sum_s \sum_{i:E_i \in n^{\text{th}}\text{ seg}} A(\ln L_m, \ln L_s(E_i)) \left|\frac{dL_s}{dE}\right|_{L_m}^{-1} j_s(E_i) \tag{22}$$

We evaluate $\left.\frac{dL_s}{dE}\right|$ at L_m since that involves an interpolation, and it is more numerically stable to interpolate that once onto L_m rather than twice onto L_i (which then would get a second interpolation via A). We can precompute a matrix that works for any flux on the E_i grid:

$$M_{s,mi} = \sum_n \begin{cases} A(\ln L_m, \ln L(E_i)) \left|\frac{dL}{dE}\right|_{L_m}^{-1} & E_i \in n^{\text{th}} \text{ segment} \\ 0 & \text{otherwise} \end{cases} \tag{23}$$

Here E_i can be replaced by the energy grid of the range table (usually E_k), which removes some interpolation in constructing $\underline{\underline{M_s}}$ but necessitates performing a smart interpolation of the incident flux onto the E_k grid. The LET spectrum is then:

$$j_L(L_m) \approx \sum_s \sum_i M_{s,mi} j_s(E_i) \tag{24}$$

If $j_s(E_i)$ is incident, rather than degraded flux, we can apply a modified $\underline{\underline{D_s}}$ matrix as well:

$$j_L(L_m) \approx \sum_s \sum_i M_{s,mi} \sum_{i'} \widehat{D}_{s,ii'} j_{s,in}(E_{i'}) \tag{25}$$

$$\widehat{D}_{s,ii'} = \sum_k A(\ln E_i\ , \ln E_k\ ) \sum_{k'} D_{s,kk'} A(\ln E_{k'}\ , \ln E_{i'}\ ) \tag{26}$$

This modification applies the interpolation from the E_i grid to the E_k grid before degrading and then back again afterwards, producing degraded flux on the E_i grid. We can also precompute $\underline{\underline{M_s}}\underline{\underline{\widehat{D}_s}}$ to repeatedly convert from incident flux spectrum to LET spectrum. Next, we will describe how to compute an SEE rate from a (degraded) proton energy spectrum or from an LET spectrum.

4. Computing the SEE Rate

The SEE rate in a part is a convolution of a laboratory test cross section and the particle flux reaching the part (the degraded spectrum). It is handled differently for protons than for ions.

4.1 Proton-Sensitive Parts

Because they produce SEE mainly by colliding with nuclei that then produce SEE via the direct ionization mechanism, the laboratory data for protons is fairly insensitive to the geometry of the part—only the number of available nuclei matters. Thus, we can begin with the relatively simpler formulation of the SEE rate for protons [[5]]:

$$r_H = \int_0^\infty j_H(E)\Omega(E)dE = \int_{\ln E_0}^\infty j_H(E)\Omega(E)Ed\ln E \tag{27}$$

Here $j_H(E)$ is the (degraded) proton differential energy spectrum and $\Omega(E)$ is a cross section. Usually, the cross section is taken to have a Weibull form:

$$\Omega(E) = \mathrm{W}_<(E) = \begin{cases} s_{lim}\left[1 - \exp\left(-\left(\frac{E-E_0}{W}\right)^S\right)\right] & E > E_0 \\ 0 & \text{otherwise} \end{cases} \tag{28}$$

The parameters E_0, W, S and s_{lim} are obtained from fits to laboratory test data. E_0 is the threshold (usually in MeV), W is the scale factor (also in MeV), S is the shape factor (dimensionless), and s_{lim} is the limiting cross section (usually in cm^2). Since the knock-on process is approximately isotropic, there is little angular dependence, and we do not need to correct for the shape of the sensitive volume.

We note that because energy spans orders of magnitude, superior numerical performance with integration routines like adaptive quadrature is obtained when integrating with respect to the log of energy.

As a discrete problem, we can write the integral as:

$$r_H \approx \sum_i \mathrm{W}_<(E_i)\Delta E_i j(E_i) \tag{29}$$

where ΔE_i is the set of trapezoidal integral weights as given in Eq. (16). We can write this as a vector dot product:

$$r_\mathrm{H} \approx \vec{g}_H^T \vec{j} \tag{30}$$

$$g_{i,H} = \mathrm{W}_<(E_i)\Delta E_i \tag{31}$$

$$j_i = j(E_i) \tag{32}$$

We can precompute and store $\vec{g}_H$ and reuse it on multiple degraded proton spectra. We can also precompute $\vec{g}_H^T \underline{\widehat{D}}_H$ and store that vector to rapidly convert any incident proton spectra into a proton SEE rate.

4.2 Ion-Sensitive Parts

Now we consider ions, which cause SEE through direct ionization. The laboratory data must be corrected for the geometry of the sensitive volume. LET is the energy deposit (mainly as ionization) per unit path

length through the sensitive volume. Laboratory data are typically taken at normal incidence through the thinnest dimension of the part, but, at off-normal incidence, there are longer path lengths through the part, which allow lower LET particles to deposit enough energy to produce an upset or other undesired effect. To correct for this, we must convolve the LET spectrum with a path length distribution, which we assume corresponds to a box-shaped sensitive volume. Because of the assumed box shape, this approach is called the right parallel piped (RPP) approximation [[6]].

The ion laboratory data provide Weibull parameters L_0, W, S and s_{lim}, where L_0 is the LET threshold in LET units like MeV/(g/cm^2), W is the weight with LET units, and S and s_{lim} have the same meaning as for protons. Based on independent knowledge of the part, we assume we know the thinnest dimension h of the part. This is the dimension through which particles passed in the normal-incidence laboratory test data. We infer that the part is upset by the amount of ionization produced as the particle traverses the part (Lh). So, in essence, the laboratory data are telling us that the cross section has this form:

$$\mathrm{W'}_{<}(Lh) = \begin{cases} s_{lim}\left[1 - \exp\left(-\left(\frac{Lh - L_0 h}{Wh}\right)^S\right)\right] & Lh > L_0 h \\ 0 & \text{otherwise} \end{cases}$$

For an arbitrary path length x, the cross section is:

$$\mathrm{W'}_{<}(Lx) = \begin{cases} s_{lim}\left[1 - \exp\left(-\left(\frac{Lx - L_0 h}{Wh}\right)^S\right)\right] & Lx > L_0 h \\ 0 & \text{otherwise} \end{cases}$$

Therefore, the upset rate should be:

$$r_{\mathrm{L}} = \frac{A_p}{s_{lim}} \int_h^{x_{\max}} \int_0^{\infty} \mathrm{W'}_{<}(Lx) j_L(L) dL\, c(x) dx \tag{33}$$

$$A_p = (ha + hb + ab)/2 \tag{34}$$

$$x_{\max} = \sqrt{h^2 + a^2 + b^2} \tag{35}$$

where $c(x)$ is the probability density function for path lengths, A_p is the projected area (given a and b, the other two dimensions of the box-shaped volume), and $x_{\max}$ is the maximum chord length. Since we are usually given s_{lim}, we often compute a and b from the aspect ratio ρ, such that $a = \rho\sqrt{s_{lim}}$, $b = \sqrt{s_{lim}}/\rho$, and $s_{lim} = ab$.

The path length (or chord length) distribution is often given in its complementary cumulative integral form:

$$c_{>}(x) = \int_x^{\infty} c(x) dx \tag{36}$$

For an RPP, an exact analytical form for $c_{>}(x)$ can be found in Luke and Buehler [[7]], and approximations are available from [[8]] and [[9]]. We prefer the Luke and Buehler exact formulation. However, we note the following:

- In Eq. (A21), there appears to be a sign error in the term $9(x^2 - v_a^2)/2$; it should be negative, not positive

- In Eq. (1), an alternate form of $C_7(x)$ is more accurate on float point machines: $C_7(x) = F(w, v_a) - F(x; v_a)$.

For those using Bradford [8], it should be noted that $hd/2$ in Eq. (6c) should, in fact, be $hd/2l$, according to a footnote in Luke and Buehler. The Bendel approximation (sometimes also attributed to Bradford) is very convenient and fast when absolute accuracy is not critical [Eq. (22)]:

$$c_>(x) = \begin{cases} 1 - \frac{x}{4h} & x \le a \\ \frac{3}{4}\left(\frac{h}{x}\right)^{2.2} & a \le x < x_{\max} \\ 0 & x \ge x_{\max} \end{cases} \tag{37}$$

This form has a small discontinuity at $x = x_{\max}$, where it jumps down to zero.

In order to use $c_>(x)$, we need to rewrite the integral for r_{L} using integration by parts:

$$r_{\mathrm{L}} = \frac{A_p}{s_{lim}} \int_h^{x_{\max}} \int_0^{\infty} \mathrm{Lw}'(Lx) j_L(L) dL \, c_>(x) dx \tag{38}$$

$$\mathrm{w}'(Lx) = \frac{d\mathrm{W}_{<}(Lx)}{d(Lx)} = \begin{cases} s_{lim} \frac{S}{Wh} \left(\frac{Lx - L_0 h}{Wh}\right)^{S-1} \exp\left(-\left(\frac{Lx - L_0 h}{Wh}\right)^{S}\right) & Lx > L_0 h \\ 0 & \text{otherwise} \end{cases} \tag{39}$$

We reverse the order of integration, introduce a new variable $L_w = L\frac{x}{h}$, and write:

$$r_{\mathrm{L}} = \frac{A_p}{s_{lim}} \int_0^{\infty} \int_L^{\frac{x_{\max}}{h} L} \mathrm{w}'(L_w h) j_L(L) c_> \left(\frac{L_w}{L} h\right) h dL_w \, dL \tag{40}$$

And finally, by convention, we have the differential Weibull in its usual form:

$$\mathrm{w}(L_w) = \frac{S}{W} \left(\frac{L_w - L_0}{W}\right)^{S-1} \exp\left(-\left(\frac{L_w - L_0}{W}\right)^{S}\right) = w'(L_w h) h \tag{41}$$

The resulting integral is then:

$$r_{\mathrm{L}} = \frac{A_p}{s_{lim}} \int_0^{\infty} \int_L^{\frac{x_{\max}}{h} L} \mathrm{w}(L_w) j_L(L) c_> \left(\frac{L_w}{L} h\right) dL_w \, dL \tag{42}$$

Recognizing that $\mathrm{w}(L_w) = 0$ for $L_w < L_0$, we can narrow the inner integral:

$$r_{\mathrm{L}} = \frac{A_p}{s_{lim}} \int_0^{\infty} \int_{\max(L, L_0)}^{\max(L\frac{x_{\max}}{h}, L_0)} \mathrm{w}(L_w) j_L(L) c_> \left(\frac{L_w}{L} h\right) dL_w \, dL \tag{43}$$

The inner integral is only non-zero when $\frac{x_{\max}}{h} L > L_0$, so we can set the lower bound on the outer integral:

$$r_{\mathrm{L}} = \frac{A_p}{s_{lim}} \int_{\frac{h}{x_{\max}} L_0}^{\infty} \int_{\max(L, L_0)}^{\max(\frac{x_{\max}}{h} L, L_0)} \mathrm{w}(L_w) j_L(L) c_> \left(\frac{L_w}{L} h\right) dL_w \, dL \tag{44}$$

For numerical integration algorithms like adaptive quadrature, improved numerical performance is achieved by taking the log of the L variables:

$$r_{\mathrm{L}} = \frac{A_p}{s_{lim}} \int_{\ln \frac{h}{x_{\max}} L_0}^{\infty} \int_{\ln \max(L, L_0)}^{\ln \max(\frac{x_{\max}}{h} L, L_0)} \mathrm{w}(L_w) j_L(L) c_> \left(\frac{L_w}{L} h\right) L_w d \ln L_w \, L d \ln L \tag{45}$$

However, since $j_L(L)$ can be rough, trapezoidal integration with respect to L can perform as well or better than adaptive quadrature. We can write the trapezoidal integral as a vector dot product:

$$r_{\mathrm{L}} \approx \vec{g}_L^T \vec{j}_L \tag{46}$$

$$j_{m,L} = j_L(L_m) \tag{47}$$

$$g_{m,L} = \begin{cases} \frac{A_p}{s_{lim}} \int_{\ln \max(L_m, L_0)}^{\ln \max(\frac{x_{\max}}{h} L_m, L_0)} \mathrm{w}(L_w) j_L(L_m) c_> \left(\frac{L_w}{L_m} h\right) L_w d \ln L_w \, \Delta L_m & L_m > \frac{h}{x_{\max}} L_0 \\ 0 & \text{otherwise} \end{cases} \tag{48}$$

where ΔL_m are the trapezoidal weights generated using the same approach as in Eq. (16). We note that there is usually little difference using ΔL_m or $L_m \Delta \ln L_m$ for the outer integral weights.

As for protons, we can store this vector, which is independent of species. We can also precompute species-specific vectors $\vec{g}_L^T \underline{\underline{M}}_s \underline{\underline{\widehat{D}}}_s$ and $\vec{g}_L^T \underline{\underline{M}}_s$ that convert from incident ($\vec{j}_{s,in}$) or degraded flux ($\vec{j}_{s,out}$) to SEE rate attributable to each species. Then the SEE rate is:

$$r_{\mathrm{L}} \approx \sum_s \vec{g}_L^T \underline{\underline{M}}_s \underline{\underline{\widehat{D}}}_s \vec{j}_{s,in} \approx \sum_s \vec{g}_L^T \underline{\underline{M}}_s \vec{j}_{s,out} \tag{49}$$

4.3 Final Notes

If all fluxes have the same number of energy grid points, a convenient approach to bookkeeping presents itself. We can assemble flux matrices $\underline{\underline{J}}_{in}$ and $\underline{\underline{J}}_{out}$ whose rows span the energy grid and whose columns span the species. We can then tabulate the vectors $\vec{g}_L^T \underline{\underline{M}}_s \underline{\underline{\widehat{D}}}_s$ and $\vec{g}_L^T \underline{\underline{M}}_s$ into matrices $\underline{\underline{H}}_{in}$ and $\underline{\underline{H}}_{out}$, respectively, whose rows span the energy grid and whose columns span the species. Then SEE rate calculation is the element-by-element multiplication $\underline{\underline{H}}_{in} \odot \underline{\underline{J}}_{in}$ or $\underline{\underline{H}}_{out} \odot \underline{\underline{J}}_{out}$, followed by a sum over all the resulting elements (rows and columns). This completes our treatment of the SEE rate calculation.

Up to this point, we have computed the SEE rate given parameters of a single sensitive volume (e.g., one bit). However, many devices have multiple instances of the sensitive volume. In such cases, the limiting cross section from the laboratory may need to be divided by the number of volumes to obtain the cross section s_{lim} for a single volume. Conversely, the SEE rate r_{H} or r_{L} needs to be multiplied by the number of devices to obtain the expected rate for the entire device. With that final detail addressed, we next turn to working examples.

5. Examples

In this section, we will demonstrate the calculations while also comparing them to the widely used CREME96 software [[10]]. We begin by computing degraded proton and helium spectra using range tables from SCREAM [[11]], NIST [[12]], and SRIM [[13]]. For these tests, the proton spectrum is an E^{-2} power law from 1 MeV to approximately 3 GeV, and the helium spectrum $E^{-2}/10$ from 4 MeV to approximately 12 GeV. Figure 1 shows that SCREAM and SRIM agree well, and that the slow (quadrature) and fast (trapezoidal) methods agree for a spherical 100 mil Al shield.

Figure 2 compares the incident and degraded spectra for a SCREAM table in a 15 mil SiO_2 slab shield. The flux is incident from only one side of the slab, meaning that the degraded spectra approach half the incident flux at high energies. The slow method uses double adaptive quadrature. The faster method uses adaptive quadrature to compute the $\underline{\underline{Q}}$ matrix but then uses the trapezoidal method ($\underline{\underline{D}}$) to perform the species-specific part of the calculation. The fastest method computes $\underline{\underline{Q}}$ and $\underline{\underline{D}}$ using the trapezoidal method. Figure 3 compares SCREAM and NIST tables for a 15 mil SiO_2 slab shield, showing good agreement.

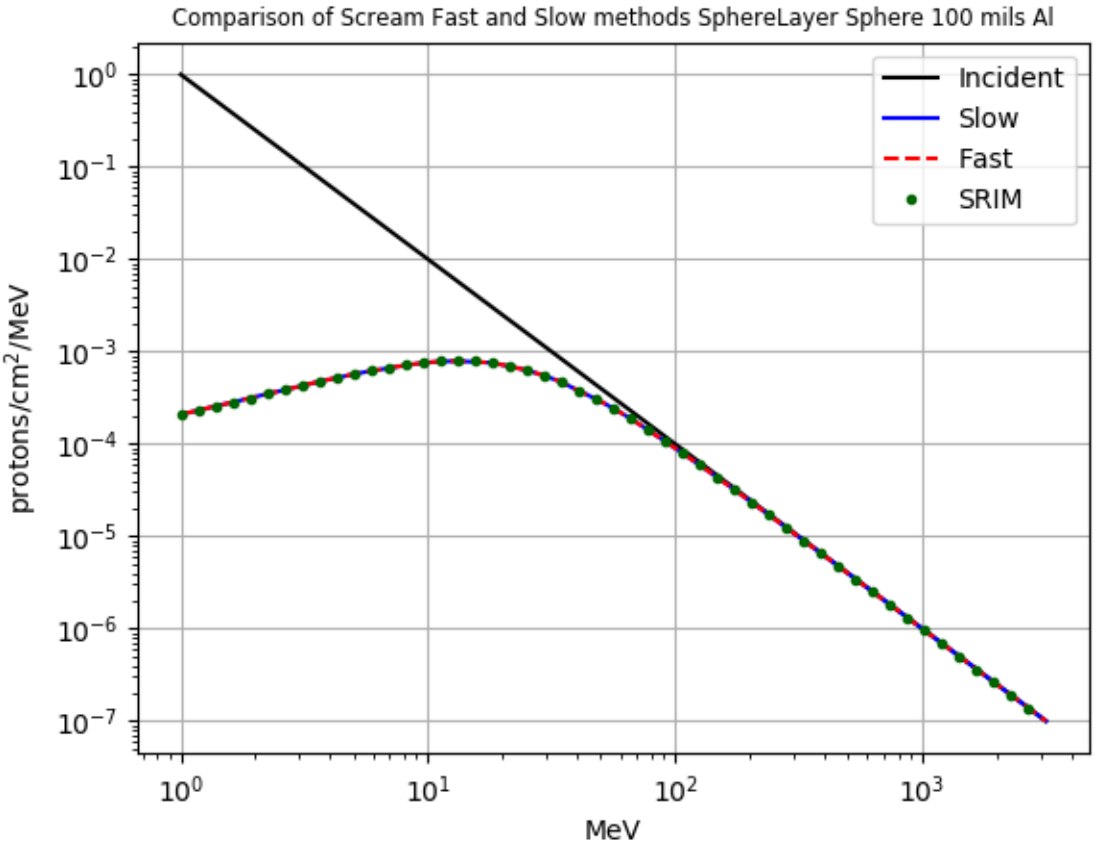

Figure 1. Incident and degraded proton spectra, using the slow (quadrature) and fast (trapezoidal) methods with a SCREAM range table, as well as the (slow) calculation for a SRIM range table. All three methods produce very similar degraded spectra. The shield is a 100 mil aluminum sphere.

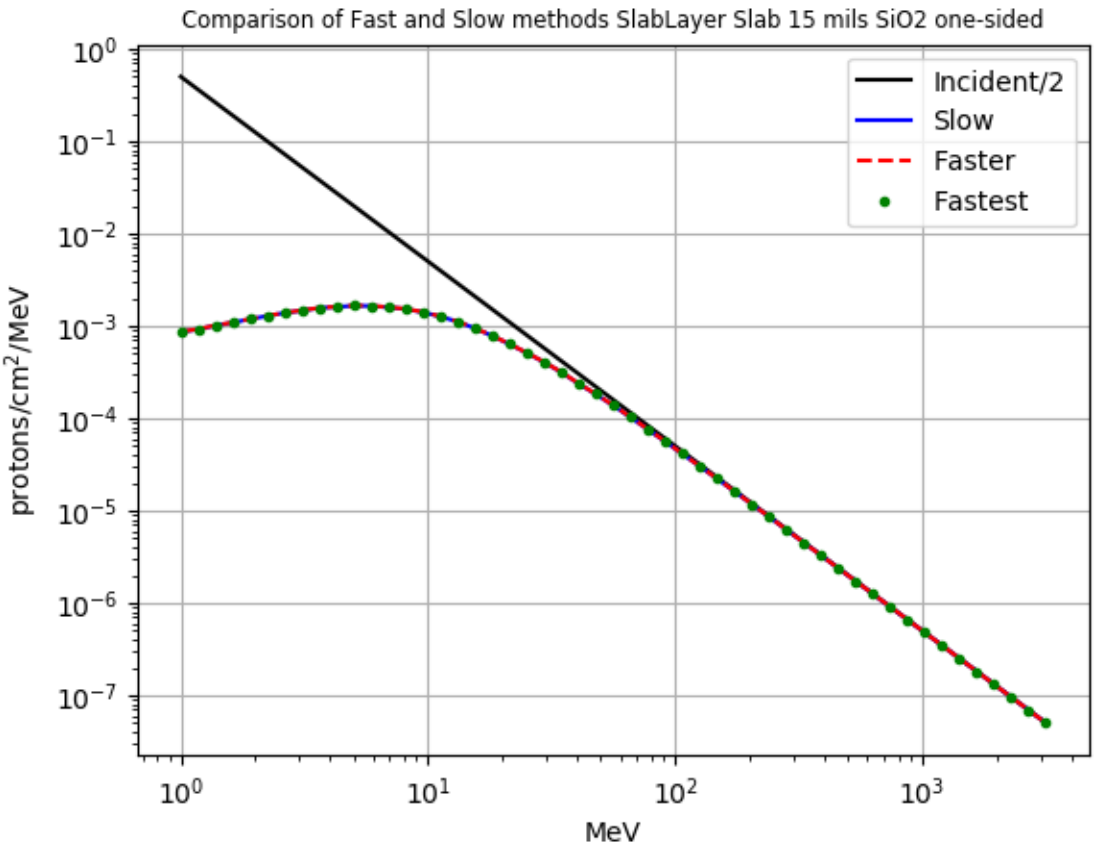

Figure 2. Incident and degraded proton spectra, using the slow (quadrature), fast (trapezoidal with $\underline{\underline{Q}}$ by quadrature), and fastest (trapezoidal $\underline{\underline{D}}$ and $\underline{\underline{Q}}$) methods with a SCREAM range table. All three methods produce very similar degraded spectra. The shield is a 15 mil SiO_2 slab with flux incident from only one side.

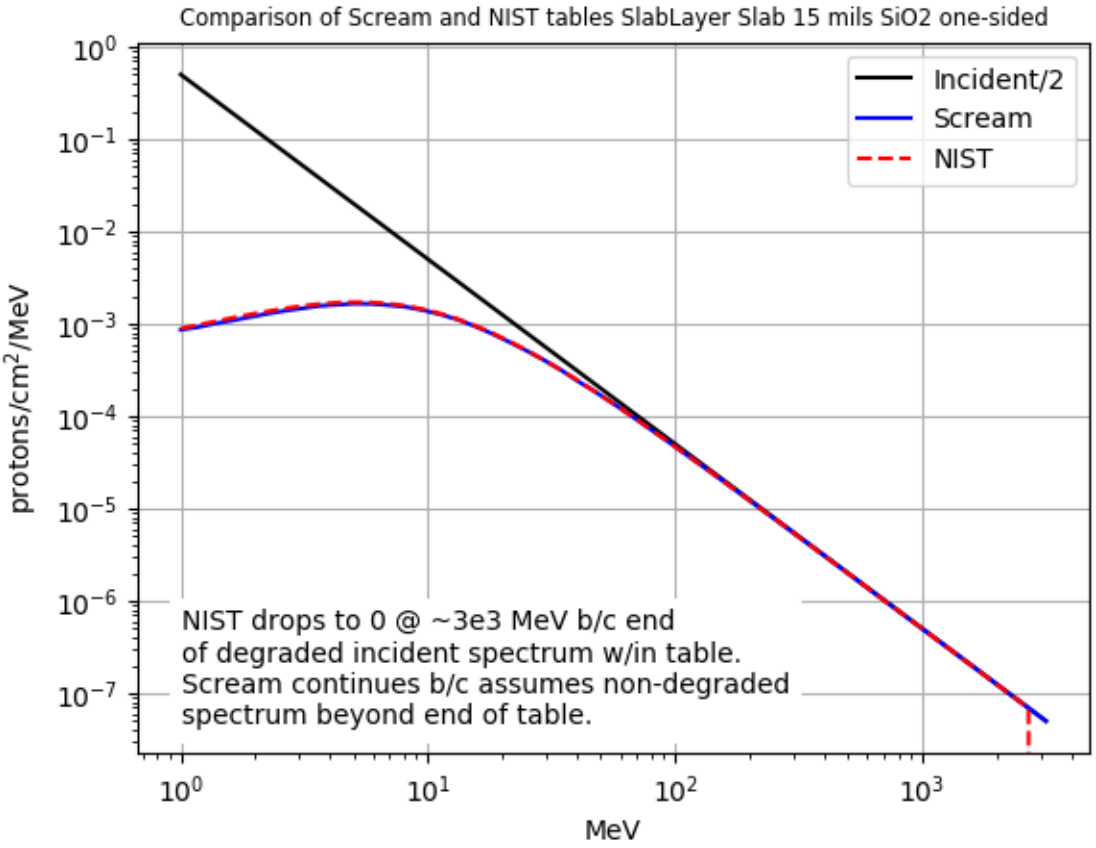

Figure 3. Incident and degraded proton spectra, using the slow (quadrature) method with SCREAM and NIST range tables. Both tables produce very similar degraded spectra. The shield is a 15 mil SiO_2 slab with flux incident from only one side.

Figure 4 shows incident and degraded spectra for protons and helium in a spherical shield. The fast and slow methods are in good agreement. Figure 5 shows the resulting LET spectrum combining the incident protons and helium spectra. Collectively, these figures show that the various methods and range-energy tables are all in good agreement.

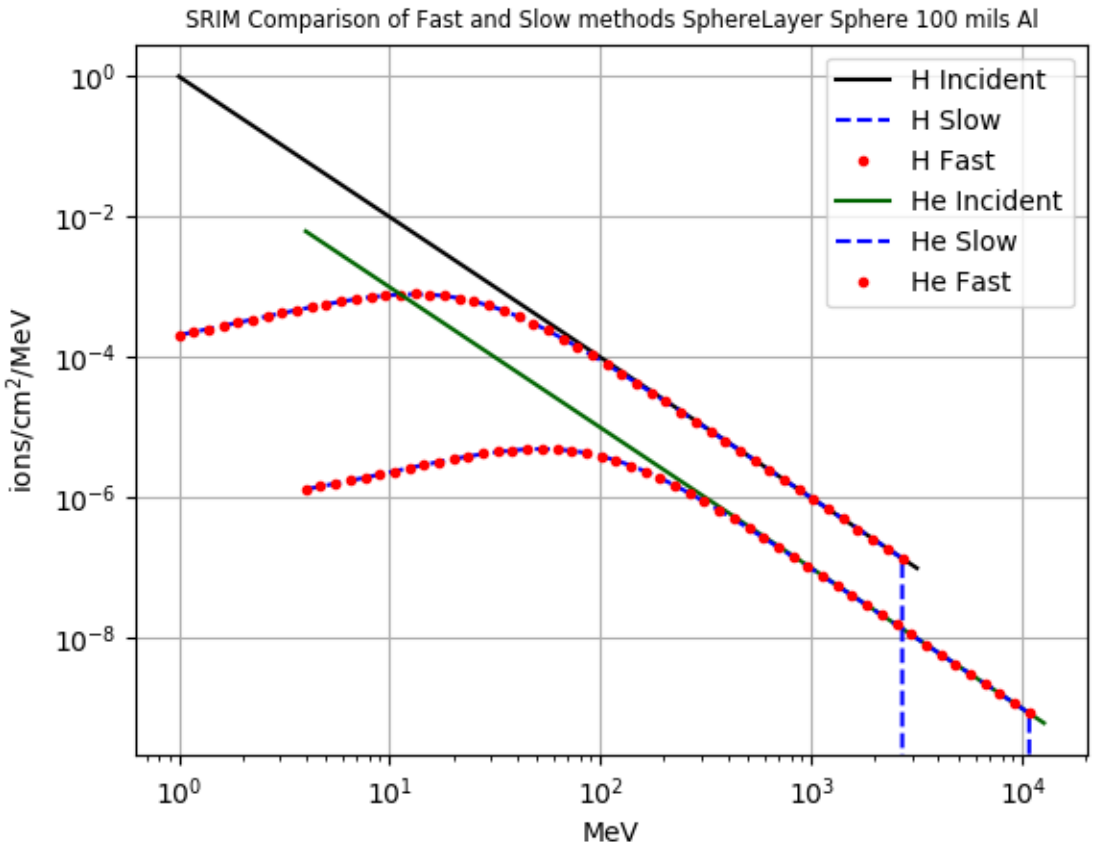

Figure 4. Incident and degraded proton and helium spectra, using the slow (quadrature) and fast (trapezoidal) methods with a SRIM range table. Both methods produce very similar degraded spectra. The shield is a 100 mil aluminum sphere.

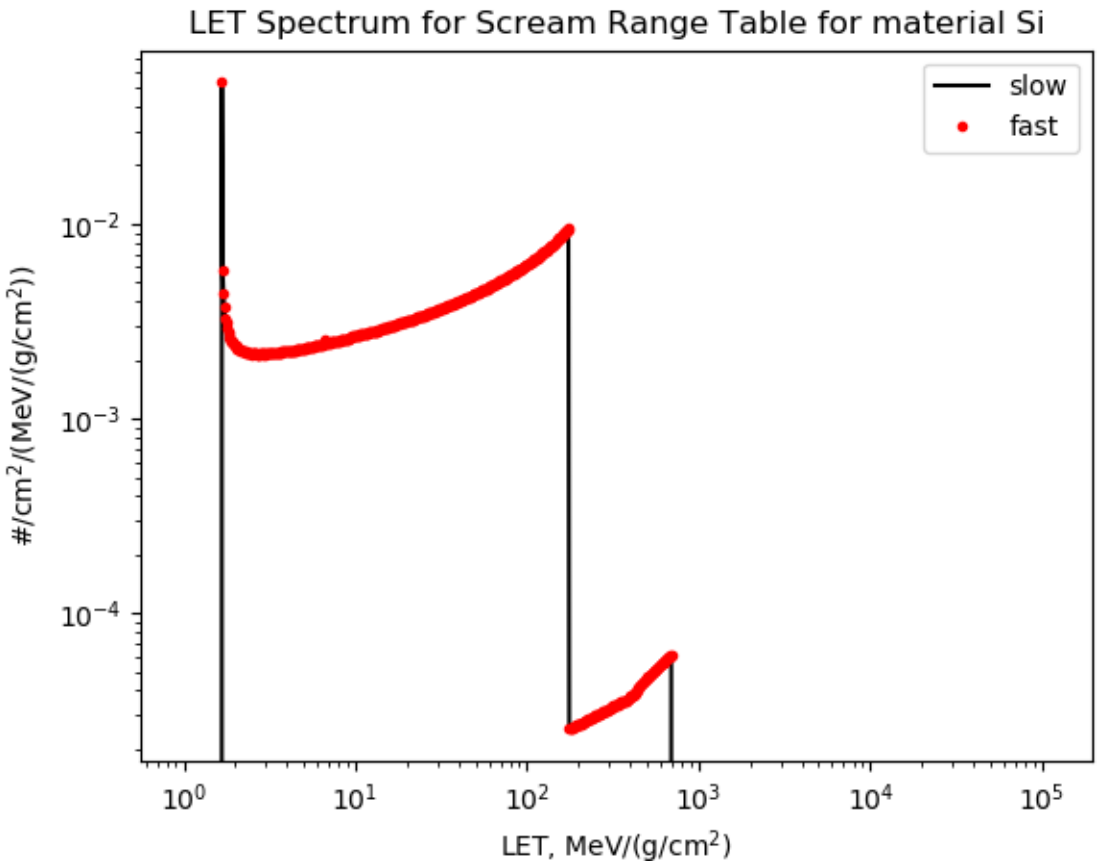

Figure 5. LET spectrum for protons and helium ions in silicon using the slow (quadrature) and fast (trapezoidal) methods using a SCREAM range table. Both methods produce very similar degraded spectra.

Next, we move on to a realistic case. CREME96 provides a combined solar and trapped spectrum for an 800 km polar orbit. We first examine a proton-sensitive part, the LM7912 voltage regulator [[14]] with E_0 = 30 MeV, W = 10 MeV, S = 1, s_{lim} = 1E-11 cm^2, and one sensitive volume. The ion energy spectrum outside the spacecraft is provided by CREME96 as a table giving an energy spectrum for each species versus normalized energy MeV/nuc, both incident flux and behind 100 mils Al spherical shielding.

The CSDA degraded spectrum is computed by both quadrature (slow) and trapezoidal (fast) methods. The incident and degraded spectra provided by CREME96, as well as the CSDA degraded spectrum using trapezoidal integrals, are shown in Figure 6. The agreement in the degraded spectra is good: the dotted lines (CSDA) and dashed lines (CREME96) fall nearly on top of each other. The SEE rate prediction results are given in Table 1. Note that we have included a case (CREME96 spectrum + trapezoidal) where the CREME96 degraded spectrum is used as input to the trapezoidal SEE rate calculation. All these methods agree to better than 1 percent.

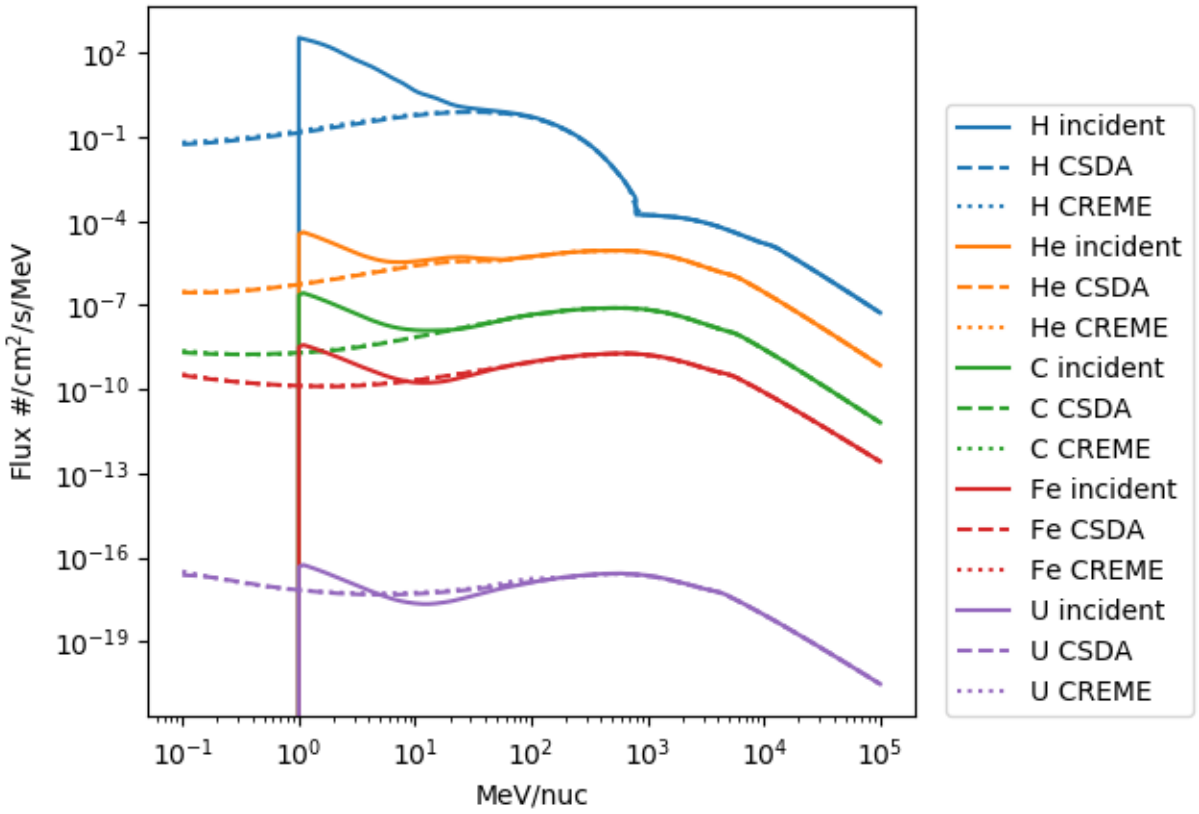

Figure 6. Incident and degraded ion energy spectra from CREME96 and the CSDA method with trapezoidal integrals.

Table 1. SEE Rates for Three Example Parts

	LM7912 - Protons	LM7912-Ions	ATMEGA1280
CREME96 Rate (SEE/s)	1.10564e-09	1.00594e-07	2.54608e-09
CREME96 Spectrum + Trapezoidal Rate (SEE/s)	1.10564e-09	6.87335e-08	2.47301e-09
Trapezoidal Rate (SEE/s)	1.10225e-09	6.35234e-08	2.35922e-09
Quadrature Rate (SEE/s)	1.10141e-09	9.42733e-08	2.1797e-09
Trapezoidal Difference from Quadrature	0.08%	-33%	8%
Trapezoidal Difference from CREME96	-0.3%	-37%	-7
Quadrature Difference from CREME96	-0.4%	-6%	-14%
CREME96 Spec. + Trapz Diff. from CREME96	0%	-32%	-3%

Finally, we turn to ion-sensitive parts. We will examine two parts: (1) the LM 7912, with L_0 = 0.5 MeV/(mg/cm^2), W = 30 MeV/(mg/cm^2), S = 1, s_{lim} = 2E-5 cm^2, and 100 sensitive volumes, a square aspect, and 1 µm thickness; and (2) the ATMEGA1280 microcontroller [[15]] with L_0 = 10 MeV/(mg/cm^2), W = 120 MeV/(mg/cm^2), S = 1.5, s_{lim} = 5E-5 cm^2, and 100 sensitive volumes, a square aspect and 1 µm thickness. First, we convert the degraded ion spectra into a unified LET spectrum, leaving out protons. Figure 7 shows fairly good agreement between the CSDA method and the more advanced method used by CREME96. There are some disagreements as to the details of the peaks, likely

attributable to different degradation approaches and different range-energy tables. The inset shows that the peak offsets are not systematically higher or lower between CREME96 and the CSDA method. (Note the abscissa units are MeV/(g/cm^2) not MeV/(mg/cm^2) as for the part Weibull parameters.)

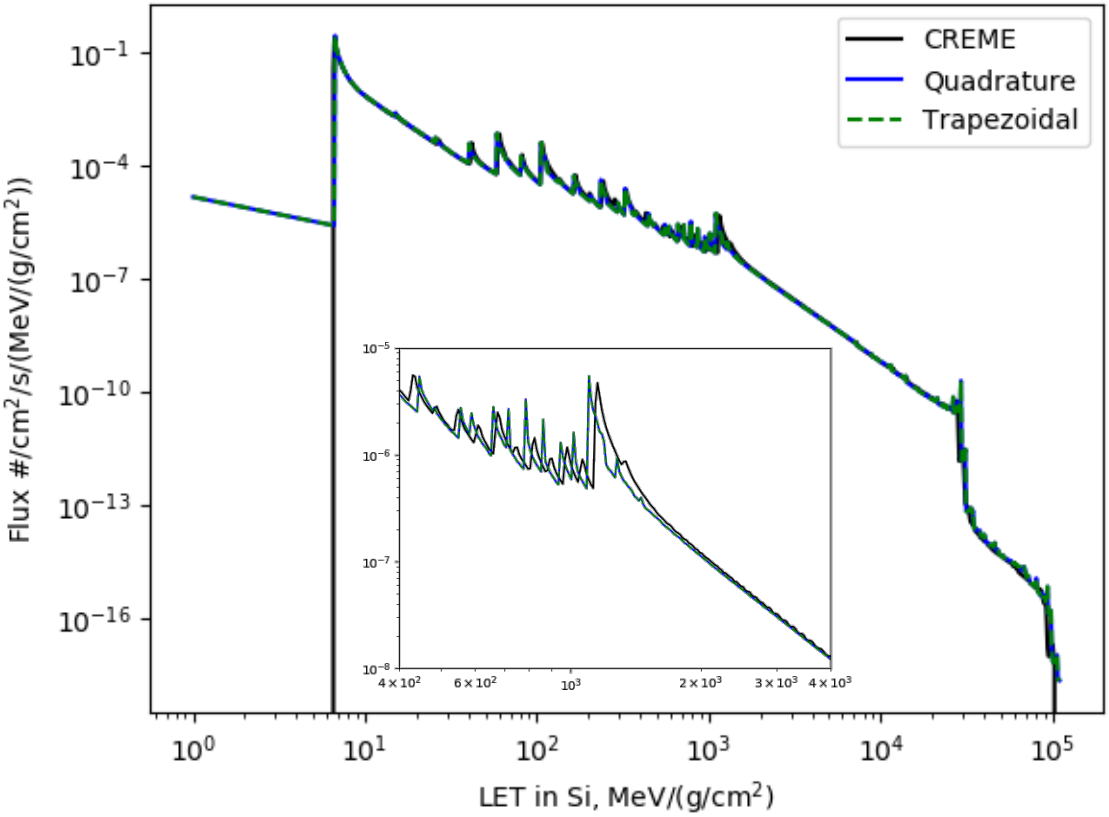

Figure 7. LET spectrum from CREME96 and CSDA method with quadrature and trapezoidal integrals.

Table 1 provides the ion SEE rate results for LM7912 and ATMEGA1280. Note that we have included a case (CREME96 spectrum + trapezoidal) where the CREME96 LET spectrum is used as input to the trapezoidal SEE rate calculation. The disagreements range from 3 to 37 percent, but there is no indication that any method is systematically biased. The disagreements appear to arise from details of the numerical scheme and differences between the CREME96 and SRIM on the LET values. For quantities that vary over many orders of magnitude, a disagreement of even 37 percent is often acceptable.

6. Summary

We have described a set of calculations that propagate incident ion energy spectra through shielding to compute the SEE rate for proton-sensitive and ion-sensitive parts. These calculations rely on the CSDA and RPP approximations. They agree well (less than 1 percent for protons and less than 40 percent for ions) with the widely used CREME96 tool, which uses different (usually more advanced) methods for computing the degraded energy spectrum and LET spectrum. The CSDA-RPP approach is suitable for qualitative analyses, and it provides the correct order of magnitude for rough quantitative analyses. Python software that implements these calculations can be found in the IRBEM-extras package of the PRBEM project at GitHub, https://github.com/PRBEM/IRBEM-extras/tree/main/csda_rpp.

7. References

[1] O'Brien, T. P., *AE9/AP9 proton single-event effects kernel utility*, Aerospace Report No. TOR-2015-02707, The Aerospace Corporation, El Segundo, CA, 2015.

[2] Petersen, E., "Single Event Effects in Aerospace," IEEE Press, Piscataway, NJ, 2011.

[3] Messenger, G. C., and M. S. Ash, "Single Event Phenomena," Springer-Science+Business Media, Dordrecht, Netherlands, 1997.

[4] Messenger. S. R. et al., "Proton displacement damage in ion dose for shielded devices in space," IEEE Trans. Nucl. Sci. 44(6), 2169, doi: 10.1109/23.659032, 1997.

[5] Petersen, E.L., "The SEU figure of merit and proton upset rate calculations," IEEE Trans. Nucl. Sci., 45(6), 2550, doi: 10.1109/23.736497, 1998.

[6] Petersen, E. L. et al., "Rate prediction for single event effects – a critique," IEEE Trans. Nucl. Sci., 39(6), 1577, doi: 10.1109/23.211340, 1992.

[7] Luke, K. L., and M. G. Buehler, "An exact, closed-form expression of the integral chord-length distribution for the calculation of single-event upsets induced by cosmic rays," J. Appl. Phys. 64, 5132, doi:10.1063/1.342420, 1988.

[8] Bradford, J. N., "A distribution function for ion track lengths in rectangular volumes," J. Appl. Phys. 50, 3799, doi:10.1063/1.326503, 1979.

[9] Bendel, W. R., "Length distribution of chords through a rectangular volume," NRL Memorandum Report No. 5369, Naval Research Lab, Washington, D.C., 1984.

[10] Tylka, A. J. et al. "CREME96: A revision of the cosmic ray effects on micro-electronics code," IEEE Trans. Nucl. Sci., 44(6), 2160, doi: 10.1109/23.659030, 1997.

[11] Messenger, S. R. et al., "Scream: a new code for solar cell degradation prediction using the displacement damage dose approach," 35th IEEE Photovoltaic Specialists Conference, June 20–25, 2010, doi: 10.1109/PVSC.2010.5614713, 2010.

[12] Berger, M. J. et al. "Stopping-power & range tables for electrons, protons, and helium ions," NIST standard reference database 124, NISTIR 4999, National Institutes of Standards and Technology, doi:10.18434/T4NC7P, 2017.

[13] Ziegler, J. F., "SRIM - The stopping and range of ions in matter," srim.org.

[14] Koga, R.; S. C. Davis; and D. J. Mabry, "Radiation Effects Testing of Selected Voltage Regulator Microcircuits with Heavy Ions and Protons," 2019 IEEE Radiation Effects Data Workshop, pp. 1-6, doi: 10.1109/REDW.2019.8906652, 2019.

[15] Davis, S. C. et al. "The Aerospace Corporation's Compendium of Recent Radiation Effect Results," 2020 IEEE Radiation Effects Data Workshop (in conjunction with 2020 NSREC), pp. 1-7, doi: 10.1109/REDW51883.2020.9325837, 2020.

AEROSPACE REPORT NO.
ATR-2022-00960

Using Continuous Slowing Down Approximation and the Right Parallel Piped Model to Estimate Single Event Effects Rates

Cognizant Program Manager Approval:

Joseph E. Mazur, PRINCIPAL DIRECTOR
PHYSICAL SCIENCES LABORATORIES
ENGINEERING & TECHNOLOGY GROUP

Aerospace Corporate Officer Approval:

Todd M. Nygren, SENIOR VP ENGINEERING & TECHNOLOGY
OFFICE OF EVP

Content Concurrence Provided Electronically by:

T Paul P. O'Brien, SENIOR SCIENTIST
MAGNETOSPHERIC & HELIOSPHERIC SCIENCES
SPACE SCIENCES DEPARTMENT
ENGINEERING & TECHNOLOGY GROUP

Technical Peer Review Performed by:

Scott C. Davis, RESEARCH SCIENTIST
MAGNETOSPHERIC & HELIOSPHERIC SCIENCES
SPACE SCIENCES DEPARTMENT
ENGINEERING & TECHNOLOGY GROUP

SY0966

AEROSPACE REPORT NO.
ATR-2022-00960

Using Continuous Slowing Down Approximation and the Right Parallel Piped Model to Estimate Single Event Effects Rates

Office of General Counsel Approval Granted Electronically by:

Kien T. Le, ASSISTANT GENERAL COUNSEL
OFFICE OF THE GENERAL COUNSEL
OFFICE OF GENERAL COUNSEL & SECRETARY

Export Control Office Approval Granted Electronically by:

Angela M. Farmer, SECURITY SUPERVISOR
GOVERNMENT SECURITY
SECURITY OPERATIONS
OFFICE OF THE CHIEF INFORMATION OFFICER

SY0966